

Describing the dispersion of plasmonic nanorod arrays via coupling of elementary excitations

Fabio Vaianella* and Bjorn Maes

Micro- and Nanophotonic Materials Group, Faculty of Science, University of Mons, 20 Place du Parc, B-7000 Mons, Belgium

(Received 18 December 2015; revised manuscript received 4 March 2016; published 15 April 2016)

Metamaterials such as metal-dielectric multilayers and cylindrical nanowires are well known, for instance because of their hyperbolic dispersion. Here we examine in detail the mode characteristics in an array of square and rectangular metallic nanorods. In particular we propose a method to describe the dispersion via the coupling of specific elementary excitations. Apparently, these fundamental modes depend on the size and shape of the nanorods, and on the particular symmetry of the Bloch modes. Specifically, we show that arrays of relatively small square nanorods are associated with coupling of single rod modes. In contrast, large nanorod arrays correspond with a basic structure consisting of four metallic corners. In the medium size case, the nature of the elementary excitation depends on the frequency range and Bloch mode symmetry. Finally, we study rectangular nanorods, which turn out to derive from a basic geometry with two semi-infinite rods. The analysis method is thus useful for a better comprehension of many other types of metamaterials.

DOI: [10.1103/PhysRevB.93.165417](https://doi.org/10.1103/PhysRevB.93.165417)

I. INTRODUCTION

Metamaterials have gained tremendous interest over the last decade thanks to their ability of controlling light in a manner impossible with natural optical materials [1–7]. These extraordinary behaviors are artificially engineered via subwavelength structures, leading to remarkable properties in left-handed media and hyperbolic metamaterials (also called indefinite media) [8–11].

Hyperbolic media provide attractive properties such as a very large density of states [12,13] and refractive index [14,15], thanks to the extreme anisotropy, leading to new light-matter interaction phenomena [16,17]. These materials turn out to be a particular case of anisotropic media, where components of the diagonalized permittivity tensor have opposite sign.

Typically, two types of structures provide for hyperbolic properties: a periodic metal-dielectric multilayer structure [Fig. 1(a)] [18–20] and an array of cylindrical metallic nanorods in a dielectric host [21,22].

Recently, Zhukovsky *et al.* showed that the hyperbolic properties in multilayer configurations arise from the plasmonic nature of the structure, and are specifically explained as the coupling of short-range surface plasmon polaritons of each unit cell [23,24]. Before, Rosenblatt and Orenstein proposed a general procedure to describe the multilayer dispersion as a competition between “gap” modes (coupling of surface plasmons through the dielectric) and “slab” modes (coupling of surface plasmons through the metal) [25]. This provides for an intuitive picture to describe the modal properties in a one-dimensional (1D) setting, by comparing the Bloch modes [judiciously averaged over the Brillouin zone (BZ)] with “elementary” structures.

In this paper we propose an extension for 2D arrays of the previously mentioned method [25]. With this extended procedure we study the dispersion of arrays of square and rectangular silver nanorods in a TiO₂ host [Fig. 1(b)]. The method is in this case more complex because of the higher number of modes and because of the 2D nature of the BZ for

the transverse Bloch components (k_x, k_y). In addition, there are more elementary modes to consider, compared to the 1D case.

We show that the dispersion of the array arises from the coupling of elementary excitations, and the particular basic structure depends on the size of the nanorods. For small and large square nanorods, the elementary geometries are a single rod and a four-corner structure, respectively. The intermediate size case arises from various elementary excitations in function of the frequency range and mode symmetry. Finally, for rectangular nanorods (one dimension much larger than the other) we find a good description via two coupled semi-infinite rods.

In Sec. II A we explain the geometries, the notation, and the analysis procedure. In Sec. III we examine the dispersion of arrays of small (compared to the period) square nanorods. In Sec. IV and V arrays of large and medium size nanorods are treated, respectively. Finally, in Sec. VI we break the symmetry between the x and y directions with rectangular nanorods, and we conclude in Sec. VII.

II. METHODS

A. Geometries

We study the dispersion of arrays of silver square and rectangular nanorods of various size in a dielectric TiO₂ host. We take the refractive index of TiO₂, $n = 2.7$, and a lossless Drude model for silver:

$$\varepsilon_{Ag}(\omega) = 1 - \frac{\omega_p^2}{\omega^2}, \quad (1)$$

with $\omega_p = 1.26 \times 10^{16}$ Hz the plasma frequency.

We slightly round the corners of the rods (via quarter circles of 1 nm radius) in order to avoid extreme hotspots for the simulations. The influence of the period is not considered here; we fix the period of all structures to $P = 30$ nm, which is much smaller than the wavelength in the range analyzed (from visible to near infrared spectrum).

For the square nanorod arrays, three cases are examined: a first case with the width w of the rods being much smaller

*Fabio.Vaianella@umons.ac.be

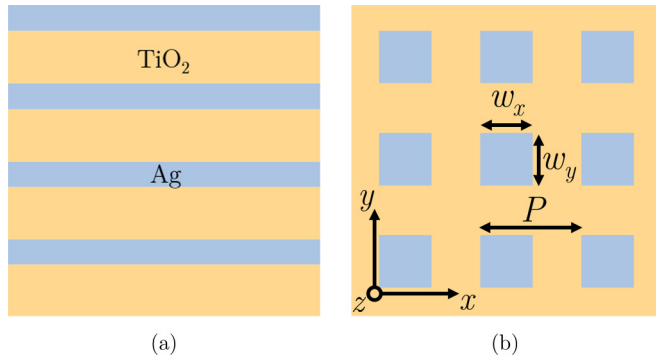


FIG. 1. (a) Multilayer consisting of periodic subwavelength layers of metal [silver (Ag)] and dielectric (TiO₂). (b) Geometry consisting of an array of square (or rectangular) silver nanorods in a TiO₂ host. w_x and w_y are the sizes of the nanorods in the x and y directions, respectively. P is the period of the array. $w_x = w_y = w$ for square nanorods.

than the period [we choose $w = 8$ nm, Fig. 2(a), analysed in Sec. III]. A second case with the width of the rods slightly smaller than the period [we choose $w = 25$ nm, Fig. 2(b), analysed in Sec. IV], and a third case with an intermediate width [we choose $w = 16.3$ nm, Fig. 2(c), analysed in Sec. V].

For these three cases the x and y directions are equivalent because the structures are invariant under rotation of 90° (the mode propagates along the z direction, out of the page here). The irreducible Brillouin zone is a triangle [Fig. 2(e)] delimited by three important points: the center of the BZ Γ where $k_x = k_y = 0$, the X_1 (X_2) point where k_x (k_y) is equal to $\frac{\pi}{P}$, and the M point where $k_x = k_y = \frac{\pi}{P}$.

We also study rectangular nanorods where we break the x, y symmetry [with x direction width $w_x = 20$ nm larger than y direction width $w_y = 10$ nm, Fig. 2(d)]. In this case, the irreducible Brillouin zone is the square delimited by the four points Γ , X_1 , X_2 , and M .

Unlike the simple multilayer case, purely transverse magnetic (TM) propagating modes do not exist here. All modes present the six components of the fields [26]. Thus it is very difficult to analytically study these lattices, and we employ the numerical software COMSOL MULTIPHYSICS 5.1, with a mode solver based on the finite element method.

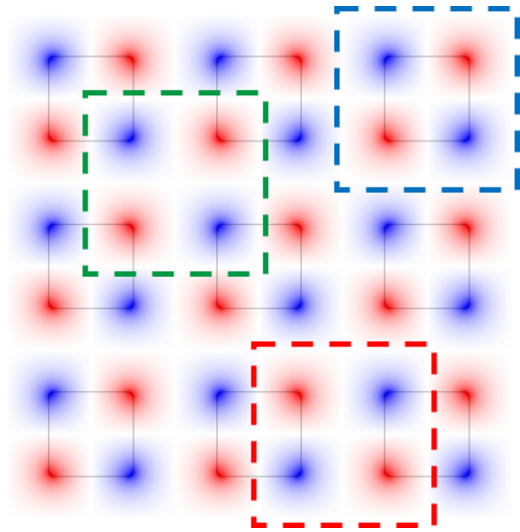


FIG. 3. The lattice under study, which can be described from different viewpoints. The blue rectangle represents single-rod excitations. The green rectangle represents four metallic corners connected via dielectric. The red rectangle is associated with structures made of two coupled (semi-infinite) rods. Shown is the z component of the electric field E_z for the aa mode (at the Γ point, $k_x = k_y = 0$) for the medium size square nanorod array at the wavelength $\lambda_0 = 700$ nm.

To obtain the dispersion of the structure, the solver calculates the modes at a given frequency and provides the propagation constant of these modes. For the periodic arrays we simulate only one unit cell of the geometry with Floquet conditions at the lateral boundaries, with predetermined values for k_x and k_y . For the elementary geometries we do not use perfectly matched layers, as the modes are confined enough and a computational width of 200 nm with scattering boundary conditions suffices.

In analogy with the multilayer case, we look for elementary excitations or “simpler” structures that can describe the array dispersions. To guide our search, the arrays can be seen as lattices with different bases (Fig. 3): a lattice of single rods (blue rectangle), a lattice of four metallic corners connected via a dielectric medium (green rectangle), or a lattice of two coupled rods (red rectangle).

The simplest excitation here is no longer the surface plasmon polariton (as for the multilayer), but the plasmonic

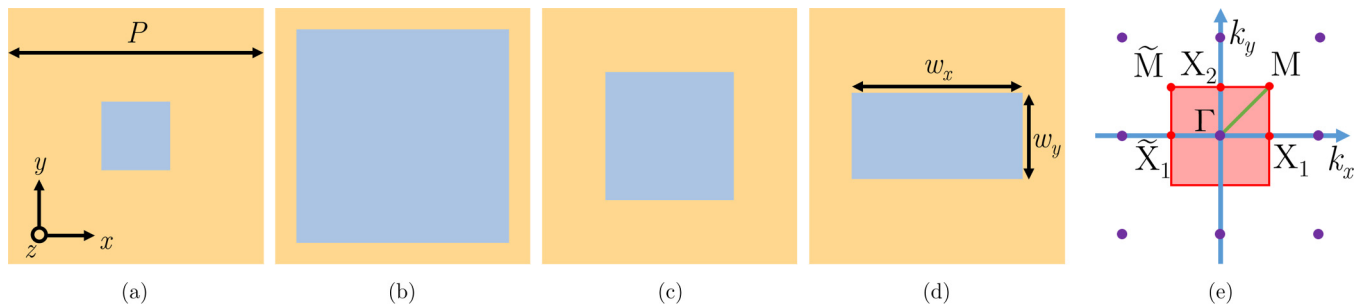


FIG. 2. Single unit cell of the structures under study: array of square nanorods with period $P = 30$ nm and nanorod width (a) $w = 8$ nm, (b) $w = 25$ nm, (c) $w = 16.3$ nm. (d) Array of rectangular nanorods of width $w_x = 20$ nm and $w_y = 10$ nm. (e) Reciprocal lattice and first Brillouin zone (in red). For square nanorod arrays, the irreducible Brillouin zone is the triangle delimited by the Γ , X_1 , and M points. For rectangular nanorod arrays, the irreducible Brillouin zone is the square delimited by the Γ , X_1 , X_2 , and M points.

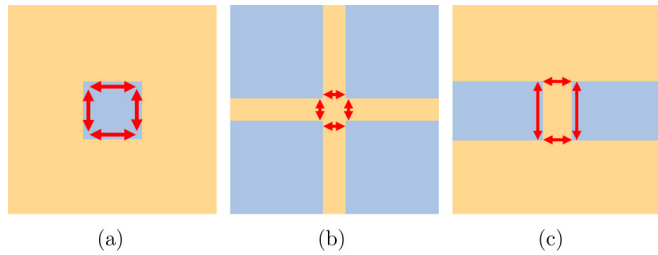


FIG. 4. Elementary structures: (a) Single rod in an infinite dielectric host. (b) Four metallic corners connected via dielectric medium. (c) Two coupled semi-infinite rods. Red arrows indicate the principal ways of coupling between corners.

mode guided by a metallic corner. This corner plasmon can couple to neighboring corners through a dielectric layer, via a metallic edge, or with a combination (through the dielectric in one direction and via the metallic edge in another direction). This leads to three elementary structures: the single-rod structure [Fig. 4(a)], the four-corner structure [Fig. 4(b)], and the coupled-rod structure [Fig. 4(c)], respectively. According to the size of the nanorods, we will see that the array dispersion seems to be associated with one of these elementary excitations. Note that various other fundamental geometries can be constructed, but analysis showed they do not corroborate well with the array modes.

B. Notations

Unlike the multilayer case, where only two different guided modes are present (a symmetric and an asymmetric one), four different symmetries for guided modes exist in our structures (Fig. 5). We use a notation similar to the one adopted in [26] to indicate the mode.

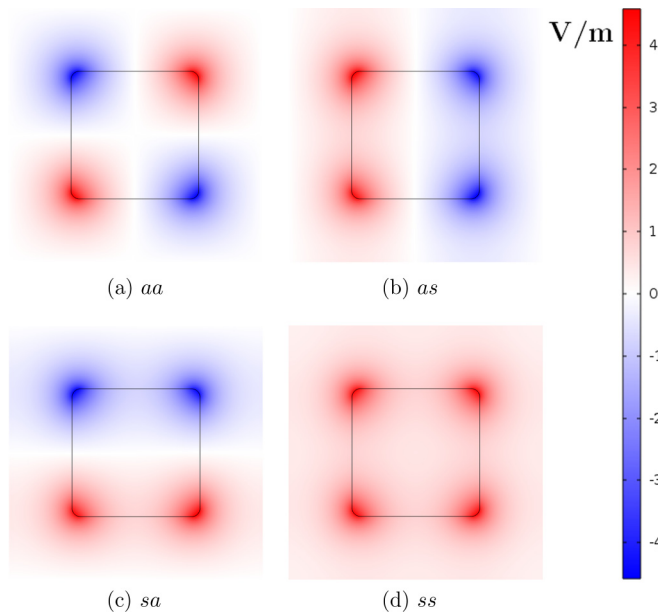


FIG. 5. E_z profiles of the electric field over a single unit cell for an array mode at the Γ point for $w = 16.3$ nm at $\lambda_0 = 700$ nm. (a) aa mode. (b) as mode. (c) sa mode. (d) ss mode.

A mode is described by two letters: the first letter represents the symmetry of E_z along a rod side in the x direction, and this letter can be “ a ” for asymmetric or “ s ” for symmetric along x . The second letter represents the symmetry along a rod side in the y direction, with the same modalities. We only focus on the lower frequency modes, so an extra notation for the order of the mode is not needed.

The four possibilities are thus the aa mode [Fig. 5(a)], as mode [Fig. 5(b)], sa mode [Fig. 5(c)], and ss mode [Fig. 5(d)]. The same nomenclature is used for the elementary structures.

Note that the sa and as modes for the arrays of square nanorods at the Γ and M points are degenerate because the x and y directions are equivalent and a rotation of 90° maps the Γ point to itself and maps the M point to the \bar{M} point, which is related via a vector of the reciprocal lattice [Fig. 5(e)]. However, the sa and as modes are not degenerate at the X_1 (or X_2) point because a rotation of 90° maps the X_1 (X_2) point to the X_2 (\bar{X}_1) point that is not connected via a vector of the reciprocal lattice.

For the elementary structures, the sa and as modes are degenerate for the single-rod and the four-corner structures, because of 90° rotation equivalence, but they are not degenerate for the coupled-rod case (no 90° symmetry).

Finally, the rectangular nanorod array modes and their elementary structure modes are not degenerate because the equivalence between the x and y directions is broken.

C. Dispersion analysis method

We introduce a 2D extension of the method used in [25]. They showed that the mean of the plasmonic band dispersion of a multilayer closely corresponds to the dispersion of elementary excitations of the structure (“slab” or “gap” modes), providing for an intuitive picture to understand the 1D array modes.

In the case of 2D arrays of square nanorods, where the irreducible Brillouin zone is a triangle, the mean of the plasmonic band is calculated as

$$\omega_m(k_z) = \frac{\omega_a(\Gamma, k_z) + \omega_a(X_1, k_z) + \omega_a(M, k_z)}{3}. \quad (2)$$

For arrays of rectangular nanorods, where the irreducible Brillouin zone is a square, we use

$$\omega_m(k_z) = \frac{\omega_a(\Gamma, k_z) + \omega_a(X_1, k_z) + \omega_a(X_2, k_z) + \omega_a(M, k_z)}{4} \quad (3)$$

with $\omega_m(k_z)$ the mean of the plasmonic band for a given propagating constant k_z . $\omega_a(\Gamma, k_z)$, $\omega_a(X_1, k_z)$, $\omega_a(X_2, k_z)$, and $\omega_a(M, k_z)$ are the frequencies of the propagating mode of the periodic array at the Γ , X_1 , X_2 , and M points, respectively.

In analogy with the 1D case, we assume that a good correspondence between the mean of the plasmonic band and the dispersion of an elementary structure indicates that the array modes “arise” from the modes of this elementary geometry. The nature of the basic structure will depend on the size and shape of the nanorods in the array. Mathematically, this assumption is simply

$$\omega_m(k_z) \approx \omega_e(k_z) \quad (4)$$

where $\omega_e(k_z)$ is the frequency of the elementary excitation for a given k_z .

One should pay attention that the symmetry of a given mode at the center of the Brillouin zone (Γ) is not necessarily the same at the X_1 and M points, so it requires caution when using Eqs. (2) and (3) to calculate the mean of the plasmonic band, and to choose the adequate elementary mode.

A detailed application of this procedure is given in the next sections.

III. SMALL NANORODS

We examine the dispersion for arrays of small (compared to the period) square nanorods with a width $w = 8$ nm. Using Eq. (2), we calculate the mean of the plasmonic band for each mode. In this case, the symmetry of each mode does not change between the Γ , X_1 , and M points.

Figure 6 shows the dispersion for the small nanorod case at each specific point of the BZ. All the modes approach the horizontal asymptote defined by $\omega = 0.255\omega_p$, which is typical for the single corner plasmon mode. This effect is because the modes are tightly confined to the corners at this frequency, so that no coupling occurs between them. As we point out in Section. II B, the sa and as modes are degenerate at the Γ and M points [red curve in Figs. 6(a) and 6(c)], but not degenerate at the X_1 point [red and magenta curves in Fig. 6(b)].

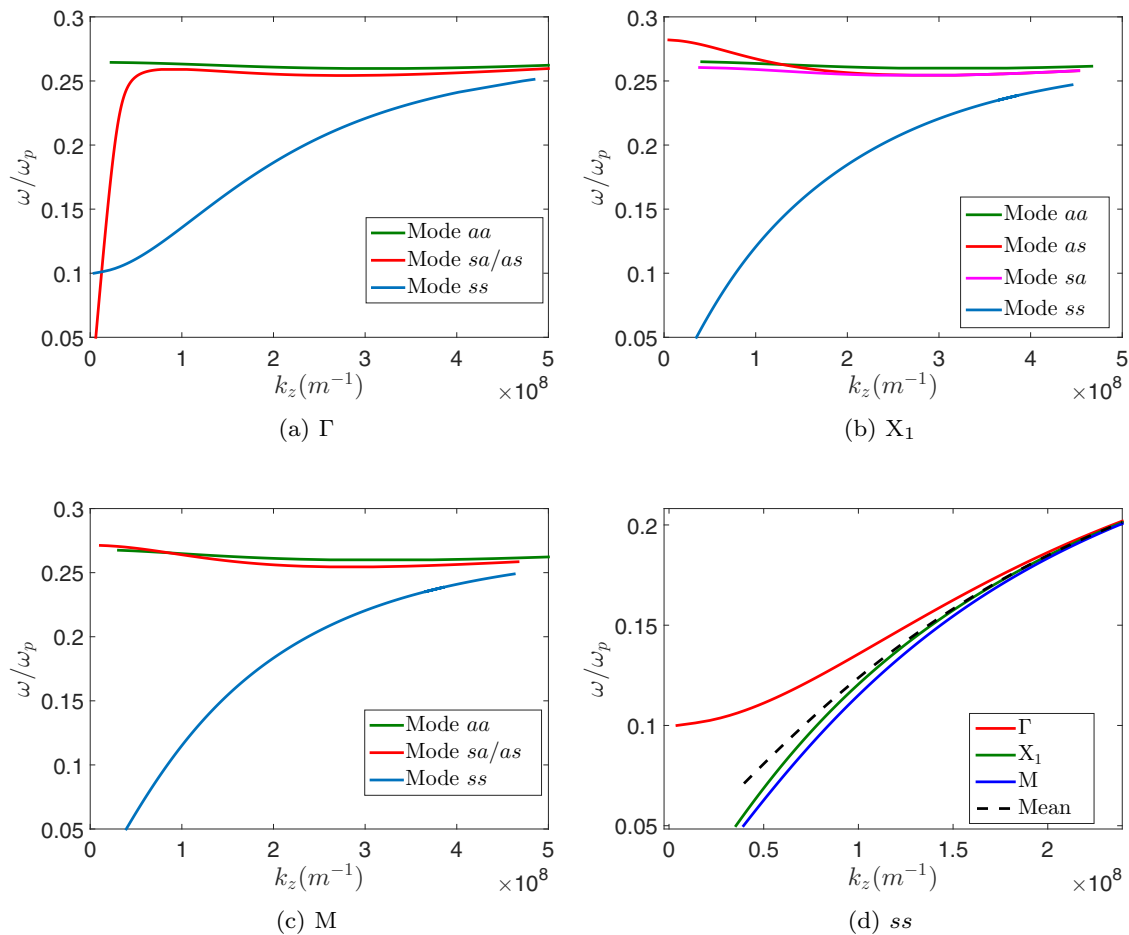


FIG. 6. Dispersion of small square nanorod array ($w = 8$ nm). (a) At the Γ point ($k_x = k_y = 0$). (b) At the X_1 point ($k_x = \frac{\pi}{p}$, $k_y = 0$). (c) At the M point ($k_x = k_y = \frac{\pi}{p}$). (d) Mean of the dispersion calculated using Eq. (2) for the ss mode (black dashed line).

Figure 6(d) shows the utilization of the procedure described in Sec. II C for the ss mode. We apply Eq. (2) to calculate the mean of the plasmonic band (black dashed curve), thus the average of the ss dispersion at the Γ [red curve, Fig. 6(d)], X_1 [green curve, Fig. 6(d)], and M [blue curve, Fig. 6(d)] points. This mean is then compared to the three elementary structure dispersions in Fig. 7(d), to determine which one best describes the array.

Now Fig. 7 shows this mean for each mode, and compares it with the three elementary modes of the same symmetry. We clearly see that the calculated mean corresponds perfectly with the dispersion of the single-rod geometry for each mode (the dashed black curve overlaps well with the blue curve).

Therefore, according to our assumption [Eq. (4)], the elementary excitation that best describes the array mode seems to be the single rod structure, which comprises four corners that are connected via metal-dielectric interfaces (the four sides of the rods). The single-rod, being the “basic” excitation, is also intuitively acceptable in these small rod arrays, as the rods are too far from each other for efficient coupling.

IV. LARGE NANORODS

We proceed with the same treatment for large square nanorod arrays ($w = 25$ nm). Again, using Eq. (2) we calculate

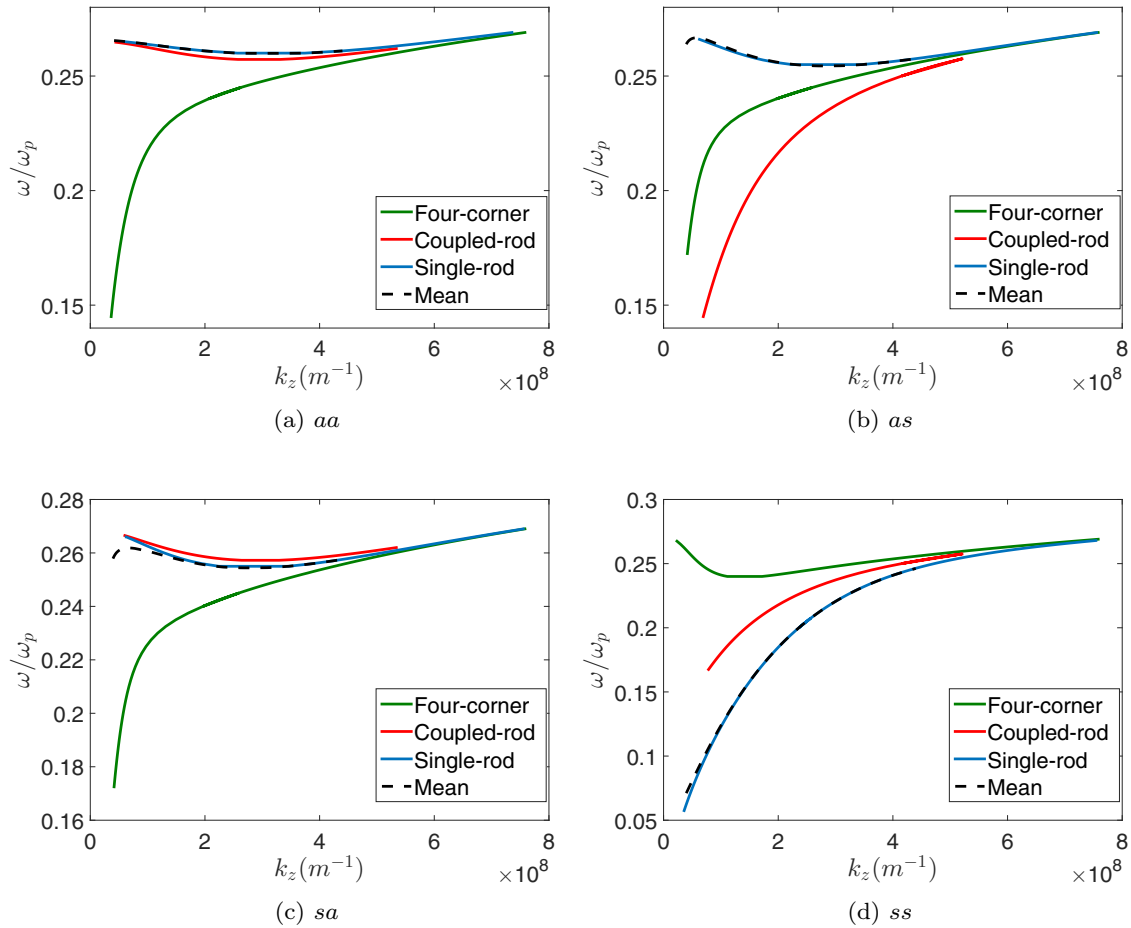


FIG. 7. Comparison between the mean calculated with Eq. (2) and the three possible elementary excitations for the small nanorod array. For each graph, the green curve corresponds to the four-corner structure, the red curve corresponds to coupled-rod, the blue curve corresponds to single-rod, and the black dashed curve correspond to the calculated mean. (a) For aa mode. (b) For as mode. (c) For sa mode. (d) For ss mode.

the mean of the plasmonic band for each mode. However, unlike the small nanorod case, the symmetry of the mode changes between the Γ , X_1 , and M points, so that the modes need to be chosen carefully to apply Eq. (2). A summary of the mode symmetry changes is given in Table I.

We see that when the wave vector in the x direction changes from $k_x = 0$ to $k_x = \frac{\pi}{P}$, the symmetry in the x direction changes from symmetric to asymmetric (and vice versa). When the wave vector in the y direction changes from $k_y = 0$ to $k_y = \frac{\pi}{P}$, the same phenomenon occurs for the y symmetry.

TABLE I. Symmetry changes for large square nanorod arrays as functions of the Bloch wave vector for a given k_z . Each row corresponds to a particular mode. This table is also valid for the medium size nanorod array above $\omega = 0.246\omega_p$.

$\Gamma(0,0)$	$X_1(\frac{\pi}{P},0)$	$M(\frac{\pi}{P},\frac{\pi}{P})$
aa	sa	ss
as	ss	sa
sa	aa	as
ss	as	aa

Figure 8 shows the mean for each mode and compares it again with the elementary excitations of the same symmetry. In this case, the calculated mean corresponds very well with the dispersion of the four-corner structure for each mode. This implies that the plasmonic mode of the large nanorod array originates from the four-corner structure, thus the plasmonic corners mainly couple through the dielectric [Fig. 4(b)].

This statement is also confirmed by the field plots of the lattice at the three specific BZ points; see for example Fig. 9 for the profiles of the aa band (first row of Table I). At the three BZ points the same pattern emerges [Figs. 9(a)–9(c)] and this pattern is very similar to the aa mode of the four-corner structure [Fig. 9(d)], which is thus the elementary excitation.

Note that the single-rod elementary structure does not at all correspond with the mean dispersion in this case: in Fig. 8 the blue curves are not aligned with the dashed black curves. This is intuitively acceptable again: for the large nanorod structure the four nearby corners communicate strongly, which thus mainly happens through the thin dielectric.

We remark that a coupling through the dielectric is accompanied by a change of symmetry in one given direction when the Bloch wave vector is equal to $\frac{\pi}{P}$ in this direction. For

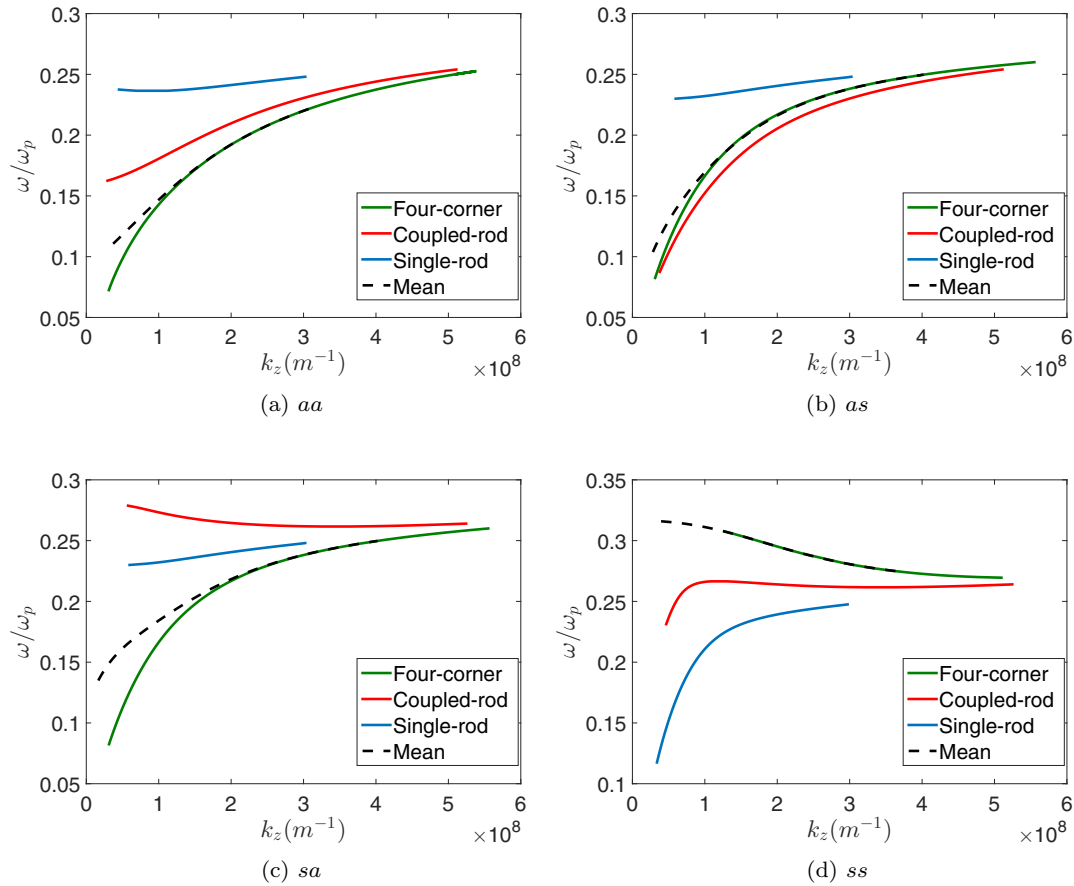


FIG. 8. Comparison between the mean calculated with Eq. (2) and the three possible elementary excitations for the large nanorod array. For each graph, the green curve corresponds to the four-corner structure, the red curve corresponds to coupled-rod, the blue curve corresponds to single-rod, and the black dashed curve correspond to the calculated mean. (a) For *aa* mode. (b) For *as* mode. (c) For *sa* mode. (d) For *ss* mode.

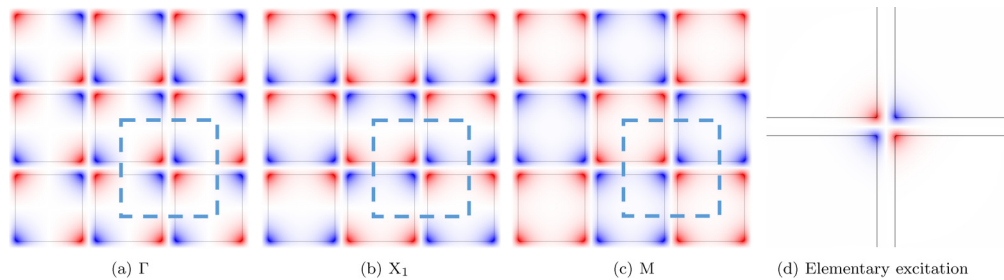


FIG. 9. E_z field plots for the *aa* band (first row of Table I) of the large nanorod array at three specific points for $k_z = 3 \times 10^8 m^{-1}$. (a) At the Γ point. (b) At the X_1 point. (c) At the M point. At the three specific points, the same pattern highlighted by the blue dashed square emerges. (d) Mode *aa* of the four-corner structure related to the large nanorod array, also for $k_z = 3 \times 10^8 m^{-1}$.

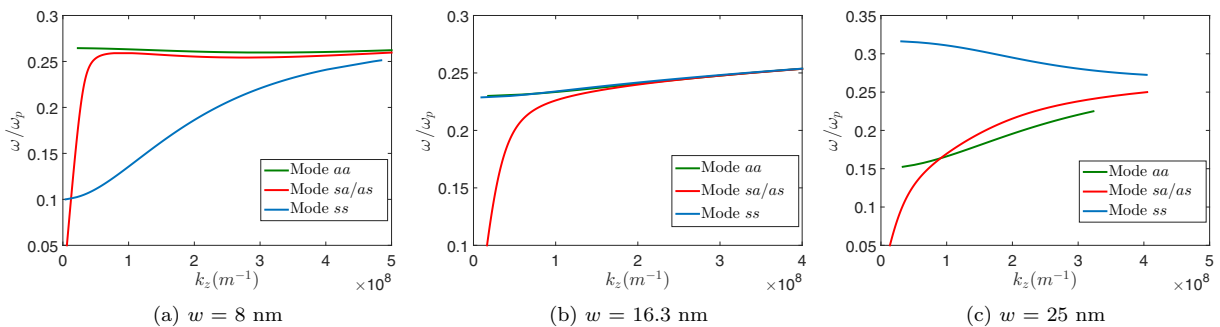


FIG. 10. Dispersion at the center of the Brillouin zone for nanorod arrays of width (a) $w = 8 \text{ nm}$, (b) $w = 16.3 \text{ nm}$, (c) $w = 25 \text{ nm}$.

TABLE II. Symmetry changes for medium size arrays below $\omega = 0.246\omega_p$ as functions of the Bloch wave vector for a given k_z . Each row corresponds to a particular mode.

$\Gamma(0,0)$	$X_1(\frac{\pi}{P},0)$	$M(\frac{\pi}{P},\frac{\pi}{P})$
<i>aa</i>	<i>aa</i>	<i>as</i>
<i>as</i>	<i>ss</i>	<i>ss</i>
<i>sa</i>	<i>sa</i>	<i>sa</i>
<i>ss</i>	<i>as</i>	<i>aa</i>

example for the first row in Table I, we see that the symmetry in the x direction of the mode *aa* changes between the Γ and X_1 points (where $k_x = \frac{\pi}{P}$) and thus *aa* becomes *sa*. When the wave vector in the y direction is equal to $\frac{\pi}{P}$, the symmetry in the y direction changes between the X_1 and M points and the mode *sa* becomes *ss*.

This change of symmetry does not happen when the coupling occurs via metal-dielectric interfaces (as for the small rod case of the previous section).

V. MEDIUM SIZE NANORODS

We study arrays of medium size square nanorods ($w = 16.3$ nm). This particular size was chosen by examining the dispersion at the Γ point for varying widths.

For small nanorods, the *aa* mode dispersion is always above the *ss* mode [Fig. 10(a), green above blue curve]. In the case

of large nanorods however, the *ss* mode is above the *aa* mode curve [Fig. 10(c), blue above green curve]. At the particular width $w = 16.3$ nm, the *aa* and *ss* curves intersect each other and the modes are very close [Fig. 10(b)].

This width thus indicates a boundary between the two regimes analyzed in the previous sections, and a mix is expected between coupling via metal-dielectric interfaces (small nanorod case) and through the dielectric (large nanorod case).

Again, using Eq. (2) we determine the mean for each mode. Here, the symmetry changes are not straightforward, because they depend on the frequency range. We delimit two frequency ranges by the intersection between the *aa* and the *sa/as* modes around $\omega = 0.246\omega_p$. Note that the *ss* and *sa/as* curves are very close but do not intersect. The symmetry changes for the two ranges are given in Table II (below $\omega = 0.246\omega_p$) and Table I (above $\omega = 0.246\omega_p$).

As we can see in the first two rows of Table II, below $\omega = 0.246\omega_p$ the modes *aa* and *as* change symmetry only in one direction (y and x direction, respectively) and, as seen before for large nanorod arrays, this is a sign of coupling through the dielectric in the y direction for the *aa* mode and in the x direction for the *as* mode (and thus coupling via metal-dielectric interface in the x direction for the *aa* mode and in the y direction for the *as* mode). The elementary excitation is thus likely to be the coupled-rod structure, and this statement is confirmed by Figs. 11(a) and 11(b).

In the third row of Table II, we notice that the mode *sa* does not change symmetry in any direction, a coupling via metal-

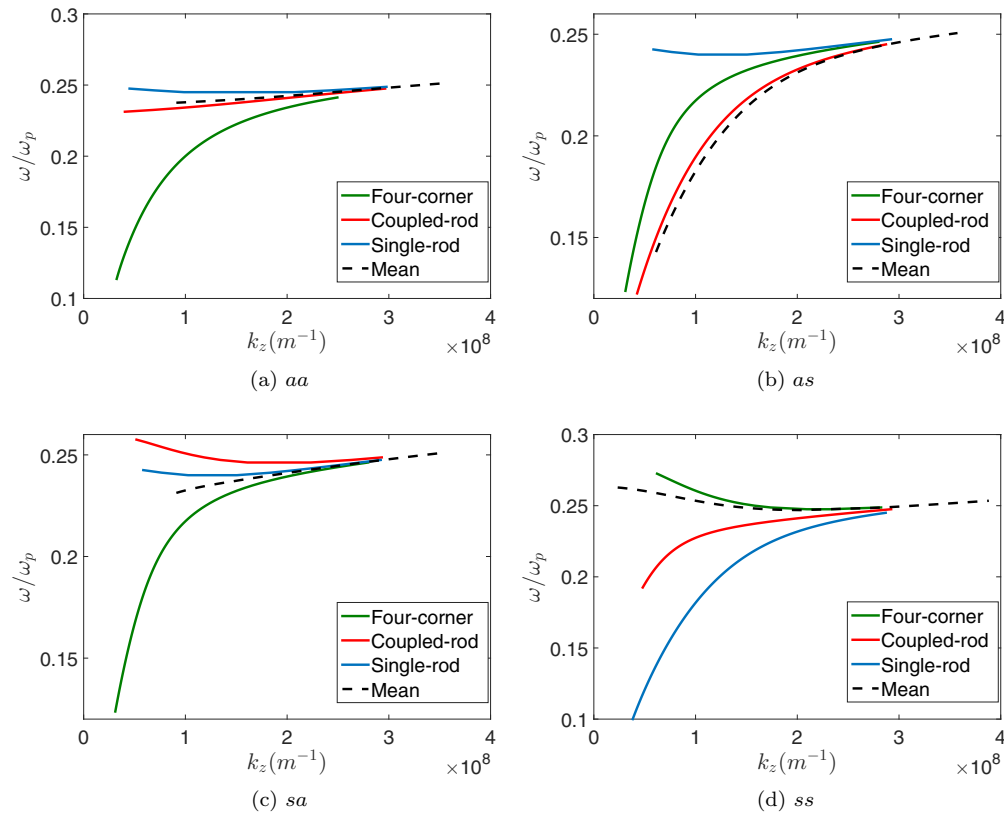


FIG. 11. Comparison between the mean calculated with Eq. (2) and the three possible elementary excitations for the medium size nanorod array. For each graph, the green curve corresponds to the four-corner structure, the red curve to coupled-rod, the blue curve to single-rod, and the black dashed curve to the calculated mean. (a) *aa* mode. (b) *as* mode. (c) *sa* mode. (d) *ss* mode.

TABLE III. Symmetry changes for rectangular nanorod arrays as functions of the Bloch wave vector for a given k_z . Each row corresponds to a particular mode.

$\Gamma(0,0)$	$X_1(\frac{\pi}{p},0)$	$X_2(0,\frac{\pi}{p})$	$M(\frac{\pi}{p},\frac{\pi}{p})$
<i>aa</i>	<i>sa</i>	<i>aa</i>	<i>sa</i>
<i>as</i>	<i>ss</i>	<i>as</i>	<i>ss</i>
<i>sa</i>	<i>aa</i>	<i>sa</i>	<i>aa</i>
<i>ss</i>	<i>as</i>	<i>ss</i>	<i>as</i>

dielectric interface occurs, and the elementary excitation is the single-rod. This statement is also confirmed with Fig. 11(c).

Finally, in the last row of Table II, the symmetry of the *ss* mode changes in the two directions, a coupling through dielectric occurs, and the elementary excitation is the four-corner structure, which is confirmed in Fig. 11(d).

Above $\omega = 0.246, \dots, \omega_p$ the dispersion is difficult to analyze from Fig. 11, as the confinement is so strong that all elementary modes converge to the single corner dispersion, so one cannot discriminate between them. However, the symmetry changes (Table I) lead us to state that the elementary excitation is the four-corner structure for all modes, because the changes of symmetry are the same as for large nanorod arrays.

At medium size, the resulting elementary excitations thus depend on the symmetry and frequency range, which is intuitively true because the coupling strengths via interfaces and dielectrics are similar. This is also indicated because the calculated average is not as perfectly superposed with the elementary modes, in contrast with small and large widths.

VI. RECTANGULAR NANORODS

Now, we break the symmetry between the x and y directions by studying rectangular nanorods instead of square ones; see Fig. 2(d). The width in the x direction is much larger than the width in the y direction. A change of symmetry of the modes between the specific points is also present in this situation and is summarized in Table III.

We note that the symmetry in the x direction changes (as in the case of large square nanorods), but not in the y direction (similar to small square arrays). The coupling between corners is thus through the dielectric in the x direction, and via metal-dielectric interface in the y direction. The leading elementary excitation is therefore the coupled-rod structure, which is confirmed by Fig. 12.

This is again intuitively acceptable because the corners are strongly connected through the dielectric in the x direction, and through the metal-dielectric interfaces in the y direction.

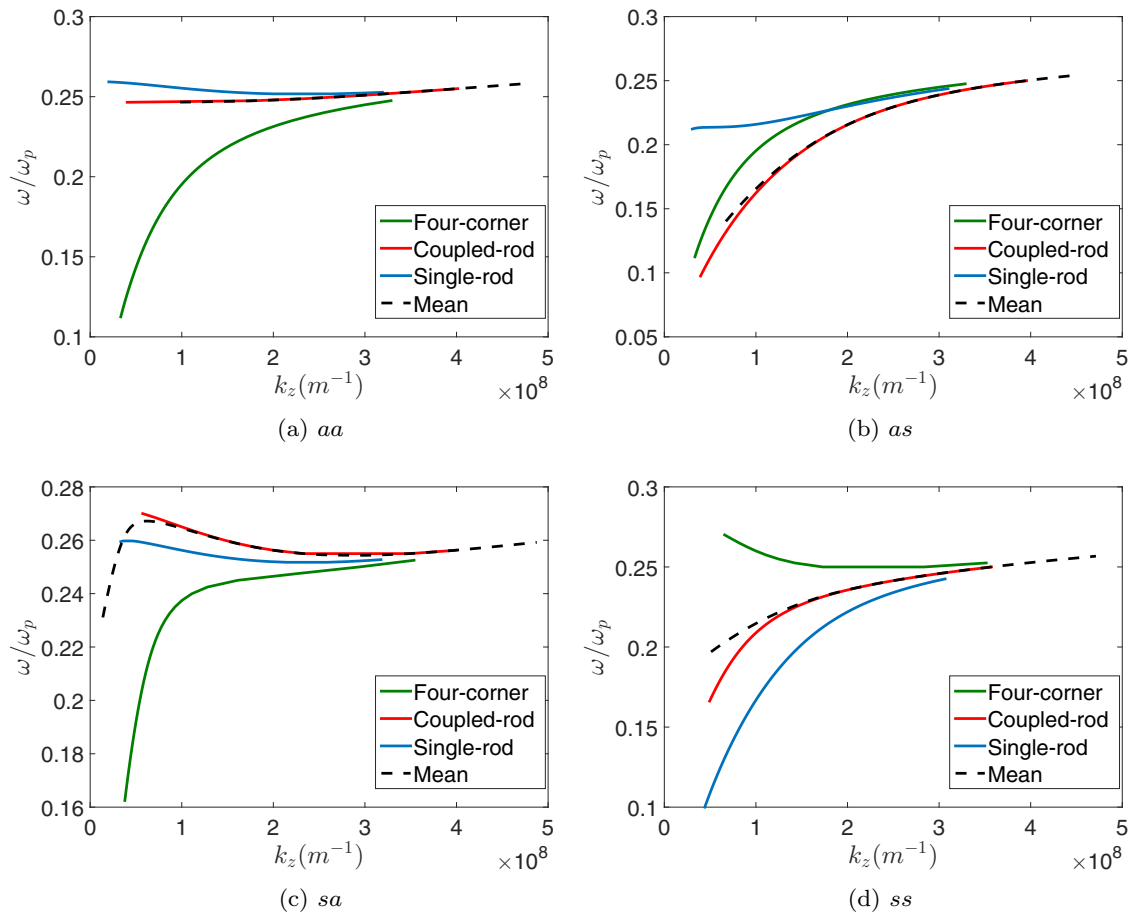


FIG. 12. Comparison between the mean calculated with Eq. (3) and the three possible elementary excitations for the rectangular nanorod array. For each graph, the green curve corresponds to the four-corner structure, the curve to coupled-rod, the blue curve to single-rod, and the black dashed curve to the calculated mean. (a) *aa* mode. (b) *as* mode. (c) *sa* mode. (d) *ss* mode.

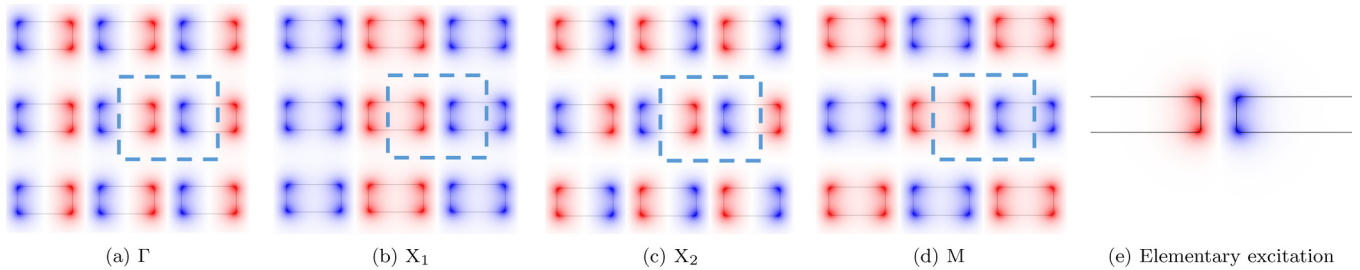


FIG. 13. E_z field plots for the as band (second row of Table III) for the rectangular nanorod array at the four specific BZ points for $k_z = 3 \times 10^8 m^{-1}$. (a) At the Γ point. (b) At the X_1 point. (c) At the X_2 point. (d) At the M point. At the four points the same pattern highlighted by the blue dashed square emerges. (e) Mode as of the coupled-rod structure related to the rectangular nanorod array, also for $k_z = 3 \times 10^8 m^{-1}$.

This can also be confirmed via the field profiles at the four BZ points; see Figs. 13(a)–13(d) for the as band (second row of Table III). The same pattern emerges, which corresponds with the as mode of the coupled-rod structure [Fig. 13(e)], thus forming the elementary excitation.

Note that the coupled-rod structure is the basic geometry in this case, because one dimension of the nanorods (w_x) is much larger than the other one (w_y), with respect to the period. If w_x and w_y were much smaller than the period, the elementary structure would be the single-rod. If both widths were close to the period, the elementary structure would be the four-corner structure.

VII. CONCLUSIONS

The dispersion of an array of square or rectangular metallic nanorods in a dielectric host can be connected directly to the modes of simpler geometries. This leading “elementary excitation” depends strongly on the size and shape of the nanorods, and can be determined via the proposed analysis method, which compares the elementary dispersion with a judiciously averaged array dispersion.

The analysis also provides information on the symmetries of the modes at the particular BZ points. In fact, a strong coupling of the corners through the dielectric in a given direction is accompanied by a change of symmetry when the Bloch wave vector in this direction is equal to $\frac{\pi}{P}$. This behavior is not observed for coupling via a metal-dielectric interface.

We demonstrated that the dispersion of small square nanorod arrays originates from single-rod excitations, and that large square nanorod arrays are associated with four-corner structures. Indeed, for small squares the corners are coupled via the metallic sides, whereas for large squares the corners couple through the dielectric.

In the intermediate size regime, the array modes result from various elementary modes, depending on the frequency and mode symmetry. This complication is due to the balanced strength of coupling via the metal sides or through the dielectric.

Finally, rectangular nanorod arrays (with one relatively large dimension) can be described by the coupled-rod structure. The corners are thus connected via the metal rod sides in the narrow direction, and through the dielectric in the wide direction.

In short, via the introduced analysis method one gains understanding of the dispersion in arrays of metallic nanorods, which opens the way to comprehend other types of metamaterials via their elementary excitations. Further work would be to exhaustively determine the coupling type in function of the nanorod dimensions, and to understand the transition between the leading basic modes.

ACKNOWLEDGMENTS

This work is supported by the Belgian Science Policy Office under the project “Photonics@be” (P7-35) and by the Fonds pour la Formation à la Recherche dans l’Industrie et dans l’Agriculture (FRRIA) in Belgium.

-
- [1] V. Shalaev and W. Cai, *Optical Metamaterials: Fundamentals and Applications* (Springer, Berlin, 2010).
 - [2] M. Skorobogatiy, *Nanostructured and Subwavelength Waveguides* (John Wiley & Sons, New York, 2012).
 - [3] B. Li and Y. He, and S. He, *Appl. Phys. Express* **8**, 082601 (2015).
 - [4] A. V. Kildishev and A. Boltasseva, and V. M. Shalaev, *Science* **339**, 1232009 (2013).
 - [5] T. Galfsky, H. N. S. Krishnamoorthy, W. Newman, E. E. Narimanov, and Z. Jacob, and V. M. Menon, *Optica* **2**, 62 (2015).
 - [6] A. A. Orlov, S. V. Zhukovsky, and I. V. Iorsh, and P. A. Belov, *Photon Nanostruct.* **12**, 213 (2014).
 - [7] W. D. Newman and C. L. Cortes, and Z. Jacob, *J. Opt. Soc. Am. B* **30**, 766 (2013).
 - [8] C. L. Cortes, W. Newman, and S. Molesky, and Z. Jacob, *J. Opt.* **14**, 063001 (2012).
 - [9] P. R. West, N. Kinsey, M. Ferrera, A. V. Kildishev, and V. M. Shalaev, and A. Boltasseva, *Nano Lett.* **15**, 498 (2015).
 - [10] E. Yoxall *et al.* *Nat. Photon.* **9**, 674 (2015).
 - [11] V. P. Drachev and V. A. Podolskiy, and A. V. Kildishev, *Opt. Express* **21**, 15048 (2013).
 - [12] O. D. Miller and S. G. Johnson, and A. W. Rodriguez, *Phys. Rev. Lett.* **112**, 157402 (2014).
 - [13] K. V. Sreekanth and T. Biaglow, and G. Strangi, *J. Appl. Phys.* **114**, 134306 (2013).

- [14] X. Yang, J. Yao, J. Rho, and X. Yin, and X. Zhang, *Nat. Photon.* **6**, 450 (2012).
- [15] D. Keene and M. Durach, *Opt. Express* **23**, 18577 (2015).
- [16] L. Ferrari, C. Wu, D. Lepage, and X. Zhang, and Z. Liu, *Prog. Quantum Electron.* **40**, 1 (2015).
- [17] J. S. Gomez-Diaz and M. Tymchenko, and A. Alù, *Phys. Rev. Lett.* **114**, 233901 (2015).
- [18] S. Feng, J. M. Elson, and P. Overfelt, *Opt. Express* **13**, 4113 (2005).
- [19] A. A. Orlov, P. M. Voroshilov, and P. A. Belov, and Y. S. Kivshar, *Phys. Rev. B* **84**, 045424 (2011).
- [20] S. V. Zhukovsky, A. A. Orlov, V. E. Babicheva, and A. V. Lavrinenko, and J. E. Sipe, *Phys. Rev. A* **90**, 013801 (2014).
- [21] J. Elser, R. Wangberg, and V. A. Podolskiy, and E. E. Narimanov, *Appl. Phys. Lett.* **89**, 261102 (2006).
- [22] N. Vasilantonakis, M. E. Nasir, W. Dickson, and G. A. Wurtz, and A. V. Zayats, *Laser. Photon. Rev.* **9**, 345 (2015).
- [23] S. V. Zhukovsky and O. Kidwai, and J. E. Sipe, *Opt. Express* **21**, 14982 (2013).
- [24] S. V. Zhukovsky, A. Andryieuski, and J. E. Sipe, and A. V. Lavrinenko, *Phys. Rev. B* **90**, 155429 (2014).
- [25] G. Rosenblatt and M. Orenstein, *Opt. Express* **19**, 20372 (2011).
- [26] P. Berini, *Phys. Rev. B* **61**, 10484 (2000).